scientific reports

Check for updates

OPEN

Compact wideband and high gain horn slot antenna array fed by printed ridge gap waveguide for X band applications

Mahboubeh Taraji[1]✉, Elham Baladi[2] & Marco A. Antoniades[1]

The design and implementation of a wideband low-loss H-plane horn slot antenna array excited by a 2-by-2 bottom-fed planar corporate feeding network is presented in this paper. The feeding network is presented by a 2-by-2 symmetric power dividing system designed to feed a 2-by-2 slot antenna array from bottom. The feeding network is realized using printed ridge gap waveguide technology as a magnetic ground, to suppress surface wave propagation and to enable quasi-TEM wave propagation along the microstrip feed. Each of the power-divider branches in the feeding network excites a slot, while maintaining the impedance bandwidth of the original unloaded power divider. The feeding mechanism and H-plane horn elements help to control the sidelobe levels and increase the overall gain. The measured results are in good agreement with the simulations, with an impedance bandwidth of over 58.5%, covering the entire X-band, with a peak gain of 14.1 dBi at 10 GHz, and a measured radiation efficiency greater than 86% throughout the operating frequency range, with a peak of 99% at 10 GHz. These are significant improvements compared to an impedance bandwidth of less than 25% and a gain of 11 dBi for the antenna array without the horn elements. The antenna has a compact size of $4.8 \times 4.8 \times 1.5\ \mathrm{cm}^2$ or $1.6\lambda_0 \times 1.6\lambda_0 \times 0.5\lambda_0$ at 10 GHz.

Keywords Printed ridge gap waveguide (PRGW), Quasi-TEM, Stopband, Slot antenna array, H-plane horn

The rapid development of wireless and satellite communication systems has led to an increasing interest in high-performance antennas at high frequency bands[1–3]. A key method for enhancing antenna performance is the use of horn elements, which offer advantages such as a simple design, high gain, wide bandwidth, and high power handling capacity. Horn antennas can be incorporated into planar structures at high frequencies, offering the advantages of planar integration[4–6], light weight and cost-effectiveness. Typically, horn antennas are designed based on the optimum horn criterion to maximize gain for a given aperture size, as the aperture size directly influences the antenna's highest achievable directivity. However, horn antennas are typically made of bulky waveguide structures, which limit their applications in planar integrated systems. Additionally, the propagation losses, fabrication cost and complexity are greater at high frequencies compared to the low-frequency bands. In array configurations with numerous radiating elements, the maximum gain is often constrained by the insertion loss of the feed network[7].

Therefore, to overcome these issues, a competition has arisen among technologies which offer lower cost, lower losses, and simpler fabrication of feeding networks. The investigation among methods to employ a promising feeding network shows that the performance of microstrip feeding networks is severely limited at high frequencies due to the high dielectric and radiation losses, significant dispersion, and surface waves[7–11]. In contrast, conventional hollow waveguide technology works effectively at higher frequencies with low radiation losses and high Q-factors; however, this comes at the cost of increased design complexity and cost as the frequency increases[12,13]. Another popular feeding network at high frequencies is substrate integrated waveguide (SIW)technology[14–16], which has electrical characteristics similar to traditional rectangular waveguides and planar configurations, such as low loss, compact profile, and easier integration with planar circuits. These properties make SIW structures more desirable than microstrip or coplanar transmission lines to design efficient antenna arrays for high frequency applications. Although SIW has a better radiation efficiency compared to its counterparts, its dielectric loss becomes problematic if it is applied to large high-gain antenna

[1]Department of Electrical, Computer and Biomedical Engineering, Toronto Metropolitan University, Toronto, ON M5B 2K3, Canada. [2]Department of Electrical Engineering, Poly-Grames Research Center, Polytechnique Montreal, University of Montreal, Montreal, QC H3T 1J4, Canada. ✉email: mtaraji@torontomu.ca

arrays[17–19]. Therefore, an alternative guiding structure, namely ridge gap waveguide (RGW) was introduced in[20] for microwave and millimeter-wave applications.

RGW structure consists of two parallel-plates: a top metal plate that acts as a perfect electric conductor (PEC), and a bottom metal plate covered with periodic textured "bed of nails" representing a perfect magnetic conductor (PMC)[21]. The air gap between these parallel plates is usually smaller than a quarter-wavelength to create a parallel-plate bandgap. By adding a wave-guiding structure, such as a ridge, between the PEC-PMC plates, a quasi-TEM mode can propagate along the guiding structure between the PMC and the top PEC plate. This waveguide has considerable advantages compared to microstrip line and SIW feed networks, including lower losses, higher power handling capability, excellent isolation properties, easy manufacturing, and easy integration, and has been used in many applications to design microwave components and devices[22–24].

The reported RGW-based antenna array solutions in the literature[25–27], suffer from the grating lobe problems, which restrict their application. In addition, loading the subarray increases the height of the antenna and adds complexity to the design. For instance, an RGW-based planar slot array antenna was presented in[25] with a maximum gain of 12.2 dBi over a frequency range of 12–15 GHz and a 21% return-loss bandwidth. The antenna size is large due to using a rectangular waveguide from the bottom plane with a complicated fabrication process of the RGW structure. A similar concept was reported in[26] at 60-GHz with a 17% return-loss bandwidth. In this case also, a transition to rectangular waveguide for excitation has increased the antenna size and using RGW has led to fabrication complexity. In[27], an array of horns was implemented on top of the slot antennas, and was excited using a classical ridge gap waveguide, termed an inverted microstrip gap waveguide, with a 10% return-loss bandwidth and a maximum gain of 25 dBi for a 4-by-4 array. However, the antenna presented in[27] suffers from high grating lobes (about -8 dB), an aperture efficiency of less than 63%, a large total size of $8\lambda \times 8\lambda$ at 10 GHz, and increased design and fabrication complexity, which is commensurate for large arrays.

The need for high-accuracy machining via computer numerical control (CNC) for the feeding layers of RGW structures, has led researchers to propose printed ridge gap waveguides (PRGW), which employ a planar structure for the design and fabrication of high-frequency integrated circuits and systems[28–31]. The notable benefit of PRGW is its standard PCB fabrication process. The textured metal nails of RGW are replaced by mushroom-like electromagnetic bandgap (EBG) structures realized using printed circuit board (PCB) implementations. Since the electromagnetic waves propagate only through the air gap, the dielectric losses in the substrate are negligible[32]. The use of PCB manufacturing techniques allows for low-cost mass production, easy integration with other circuit components, such as filters and antennas, and facilitates the development of highly integrated systems.

In this paper, we present PRGW based planar 2-by-2 H-plane horn array antenna with wide impedance bandwidth and high efficiency. The radiating performance of the antenna is improved for operation at X-band (8–12 GHz), which is suitable for telecommunication and biomedical systems. We have employed a new symmetric feeding mechanism in this work, which eliminates the need for a complicated microstrip transition design, and results in a more compact and efficient antenna. T-shaped ridges under the slots are used to enhance the impedance matching and achieve a wide impedance bandwidth over the entire X-band. Subsequently, directive H-plane horn elements are placed above the slots to improve the antenna gain with sidelobe levels below -15 dB and -10 dB for the E- and H-planes, respectively, while the overall impedance bandwidth of the antenna is optimized. Additionally, physical insight into the antenna design is provided throughout the design process. In contrast to the works presented in[25–27,33,34], the antenna proposed here has many significant advantages in terms of size, return-loss bandwidth, and far-field characteristics, and introduces a very simple configuration with low complexity in terms of design and fabrication. Table 1 shows a comparison between the measurement results of the proposed array antenna and some array antennas reported in[25,27,33,34]. The slot array antenna presented here has the widest bandwidth, highest gain, and smallest size between the mentioned antennas in Table 1.

The paper is organized as follows: First, the main design concept of the PRGW technology is discussed and the dispersion analysis using the Ansys HFSS eigen-mode solver is presented. Then, the design and simulation of a 2-by-2 PRGW feeding network, and the design procedure of the 2-by-2 H-plane horn slot antenna array are described. Next, the experimental results including return loss, gain, efficiency, and radiation patterns of the proposed antenna are presented. Finally, conclusions are drawn.

Unit cell analysis and stopband studies

PRGW structures are typically used to form a stopband to prohibit the propagation of electromagnetic waves in unwanted directions and to allow the propagation of a quasi-TEM wave along the ridge. The principal step to generate a stopband in a desired frequency range is to first determine lower and upper limits of the operating frequency band., Then, the frequencies that define the stopband region can be considered as a function of the geometric parameters of the airgap and the periodic structure[35].

Ref.	Array type	Feed network	Impedance bandwidth	Radiation efficiency	Gain	Total size
[25]	2-by-2	RGW	21% at Ku-band	NA	12.2 dBi (4 elements)	$7 \times 7 \times 2$ cm^3
[27]	4-by-4	IMGW	10% at X-band	70%	25 dBi (16 elements)	$24 \times 24 \times 4$ cm^3
[33]	2-by-2	Waveguide	10% at X-band	NA	13.8 dBi (4 elements)	$6.5 \times 6.5 \times 2.7$ cm^3
[34]	2-by-2	SIW	13% at X-band	NA	10.9 dBi (4 elements)	$11 \times 11 \times 0.32$ cm^3
This work	2-by-2	PRGW	58.5% at X-band	86%	14.1 dBi (4elements)	$4.8 \times 4.8 \times 1.5$ cm^3

Table 1. Comparison of the proposed array antenna with some reported array antennas.

In Fig. 1a, the dispersion diagram of an infinite periodic structure without a ridge has been evaluated and demonstrated. The unit cell is printed on a Rogers 5880 substrate with $\varepsilon_r = 2.2, \tan\delta = 0.0009$ and thickness $t = 1.575$ mm. The dispersion diagrams are obtained using the Ansys HFSS Eigenmode solver. It is noticeable that a wide stopband appears from around 7 to 13 GHz to prohibit surface waves from propagating in the X band. As shown in Fig. 1b by adding a microstrip line to the periodic structure, a quasi-TEM mode appears between the conducting microstrip line (green printed ridge) and the top metal plate (removed for clarity). The dispersion diagram in Fig. 1b comprising the first nine modes, illustrates the realized bandgap of the periodic structure over 7.6–13 GHz. The rectangular waveguide modes below 7.6 GHz are perturbed by the presence of the ridge. Besides, another mode appears at 13 GHz as a higher-order parallel plate mode. Thereby, the dimensions for the parameters specified in Fig. 1c are chosen in order to generate a stopband covering the whole X-band.

Symmetric feeding network

To design the 2-by-2 planar corporate feeding network, first we designed the PRGW structure to work in the X-band, as described in previous section. Then, we designed a 2-by-2 power dividing network using microstrip feed lines, and a T-shaped section was used at the end of each feed line section to obtain better impedance matching, as shown in Fig. 2a, b. The usual excitation technique for a 2-by-2 corporate feeding network in PRGW technology is using a transition mechanism from the edge of the board. This technique shown in Fig. 2a, besides adding more losses, especially due to scattering at the connection point of the PRGW and the transition, causes extra design and manufacturing complexity and reduces the frequency bandwidth. Moreover, direct input coupling between the microstrip feed line and the radiating elements breaks the elements' symmetric excitation and creates higher side-lobes. In Fig. 2b , we have incorporated a new method of excitation using a coaxial feed from the bottom of the board. This is inherently a symmetric excitation, resulting in a more compact structure, while eliminating the aforementioned-coupling and parasitic scattering issues associated with the technique shown in Fig. 2a . When a conventional feeding mechanism is used, the slots are not excited uniformly and symmetrically. The field distribution on one slot is different from its neighbour, and the fields do not have the ideal TE_{10} mode distribution on each of the slots. This is because a) the slots have different distances from the input feed line, and b) some slots are excited directly from the edges of the power guiding lines instead of being fed by the T-shaped feed section right below the center of the slot. This affects the field distributions on the slots and creates undesired modes, which has the consequence of unwanted sidelobes and a degradation of the main far-field beam. However, in our proposed feeding mechanism, all slots are fed in a similar fashion from the same T-shaped impedance matching section below the center of each slot. Both the unwanted modes due to indirect

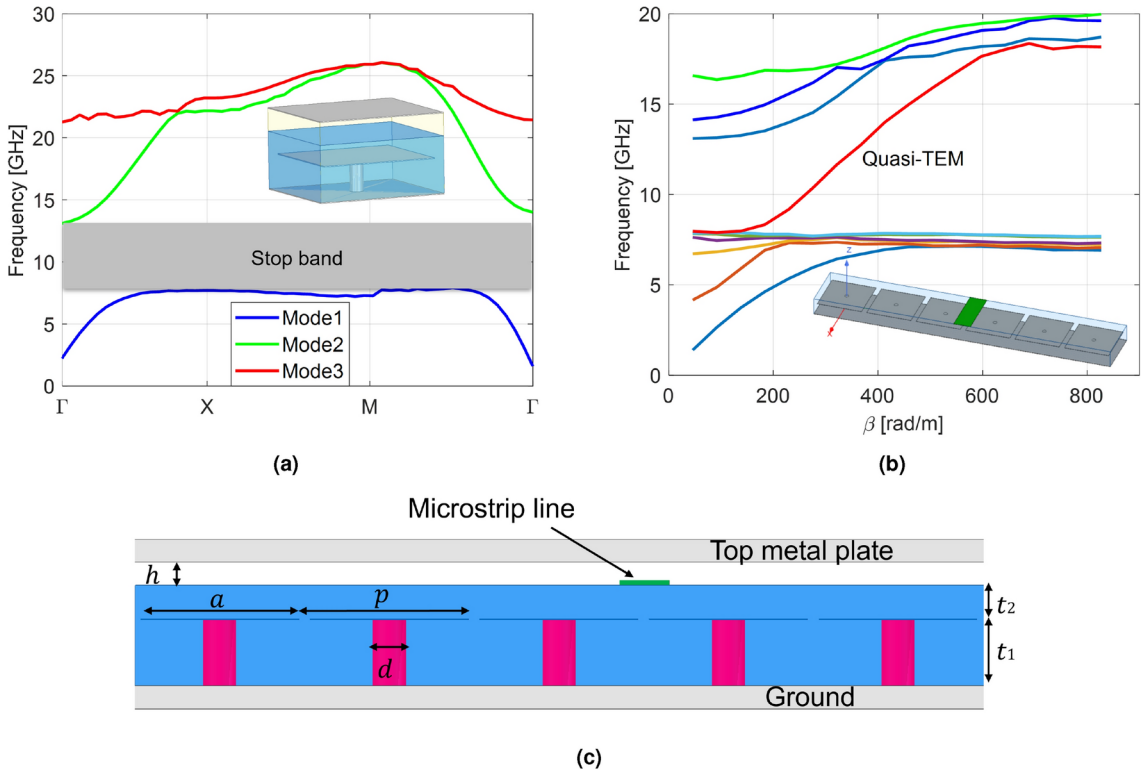

Fig. 1. Dispersion diagrams of (**a**) infinite periodic unit cell, indicating its stop band, (**b**) finite parallel-plate PRGW structure including a microstrip line of width 1 mm as a ridge, (top metal plate is removed for clarity). (**c**) Geometry of the periodic pattern. The dimensions are $h = 0.5$ mm (gap height), $d = 0.76$ mm (via diameter), $a = 3.55$ mm (patch width), $p = 3.8$ mm (patch periodicity), $t_1 = 1.575$ mm, and $t_2 = 0.778$ mm.

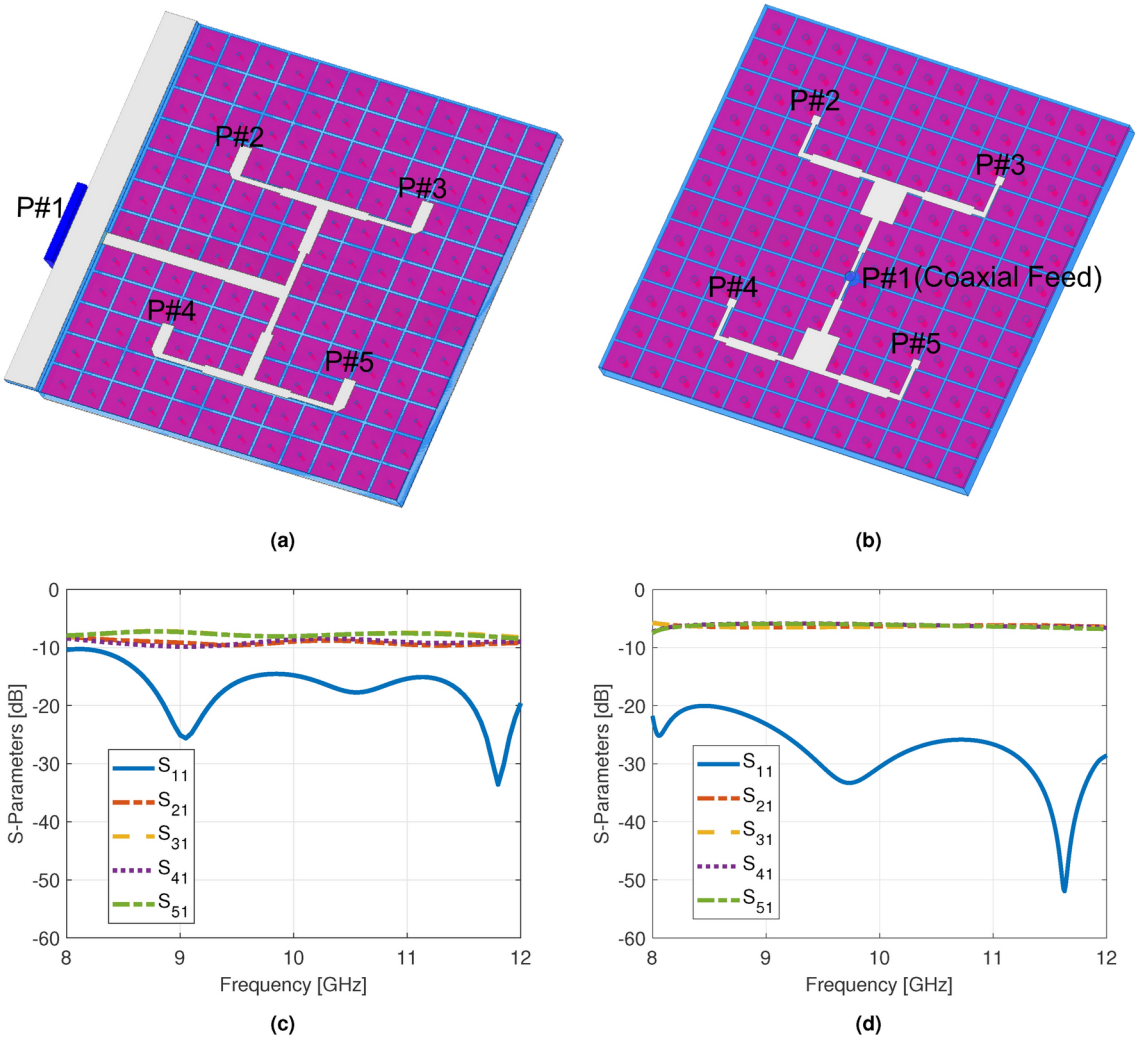

Fig. 2. Geometry of the 2-by-2 PRGW corporate feeding network excited from (**a**) the edge of the board at Port#1 (P#1), and (**b**) the bottom of the board at P#1 using a coaxial feed. The top metal plate has been removed to show the feeding structure. (**c**) S-parameters of the 2-by-2 PRGW corporate feeding network excited from the edge of the board. (**d**) S-parameters of the 2-by-2 PRGW corporate feeding network excited from the bottom of the board.

coupling (from the power guiding section) and the non-uniform excitation of the slots are eliminated. This results in increased energy directed towards the main lobe, leading to increased antenna gain, and a reduction of the sidelobes compared to the conventional feeding method.

The RF input is applied from the bottom through a coaxial feed using a 50 Ω SMA panel mount Jack connector with a 4-hole flange (Amphenol RF, Part#132108), soldered to the signal line, which then splits the power into the two main microstrip branches. Then, the next two power dividers are used to equally split the wave along each of the four smaller feed networks with equal phase, denoted as ports number 2–5 (P#2–5) in Fig. 2b . The matching at each section is obtained by using multiple stepped microstrip line impedance transformers. The S-parameters of the microstrip-PRGW transition branches of the planar feeding networks shown in Fig. 2a, b are illustrated in Fig. 2c, d , respectively. Comparison of these two plots verifies that our presented method of excitation from the bottom of the board removes the parasitic scattering issues related to the transition from the edge of the board, and demonstrates a wide impedance bandwidth covering the whole operation frequency with an input reflection coefficient less than − 20 dB ($S_{11} \leq -20$ dB), and $S_{ij} = -6$ dB, where $j = 1$, and $i = 2, 3, 4$, and 5.

Design of H-plane horn slot antenna array

The proposed antenna based on PRGW contains four layers which are illustrated in Fig. 3a . Layer 2 acts as an artificial magnetic conductor (AMC) consisting of a mushroom-like EBG connected by vias through a Rogers 5880 substrate (shown in the light-blue colour) to its ground plane on Layer 1. The microstrip feeding network described in Section III is located on Layer 3 on top of a second Rogers 5880 substrate (also shown in a light-blue colour). Figure 3b shows the details of the 2-by-2 corporate feed network design. We designed microstrip

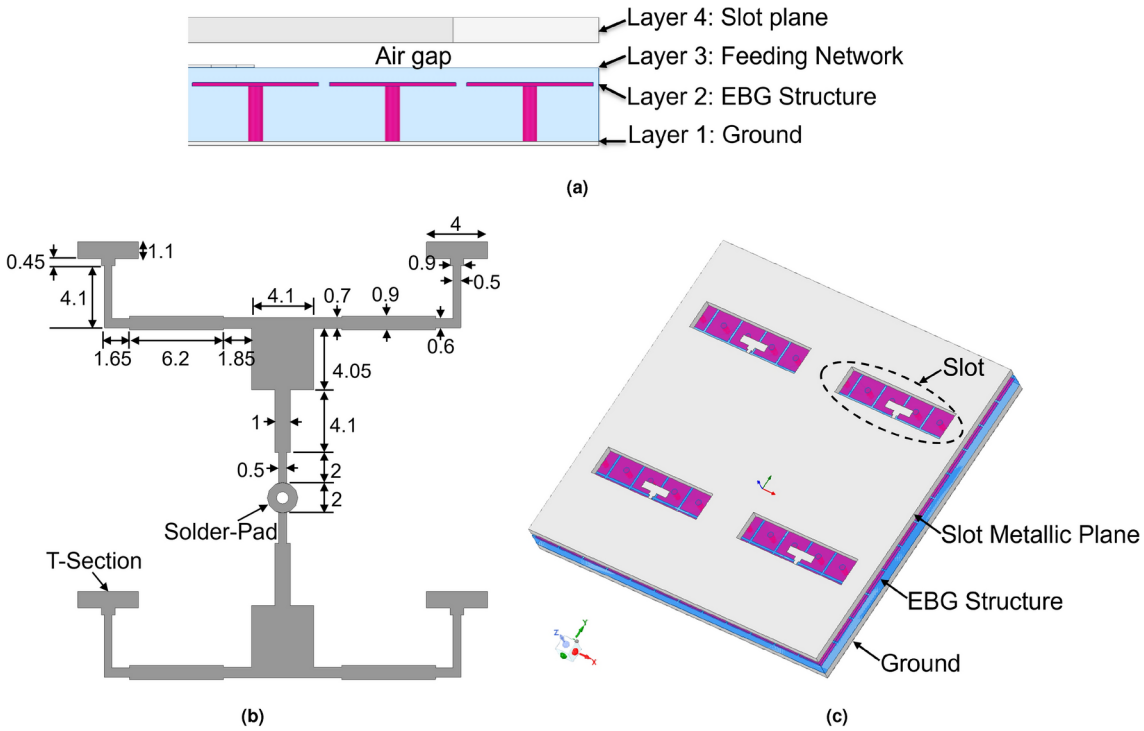

Fig. 3. (**a**) Indicated constituent layers used to realize the PRGW structure. (**b**) Geometric details of the 2-by-2 corporate feed network (dimensions are given in mm). (**c**) Diagram of the complete slot antenna array fed by the PRGW feed network.

feed lines with different lengths and widths, and we added a T-shaped section at the end of each feed line section under the slot apertures to obtain better impedance matching. There is a limitation regarding the spacing between adjacent elements. In broadside arrays, the distance between adjacent elements should be less than λ_0 to avoid of grating lobes. Here, we selected six rows of patches between adjacent elements. Therefore, we designed a 2-by-2 element array excited with equal amplitude by a symmetric feeding network with an element spacing of 23 mm, which is about 0.76 λ_0. The microstrip feed network is separated from the slot plane in Layer 4 by a 0.5 mm air gap. All parameters were first designed in Keysight-Advanced Design System (ADS) and then optimized using an Ansys-HFSS full-wave analysis. Since the field propagates in the air gap, the free-space wavelength at 10 GHz was considered for the initial ADS design. Furthermore, a pad was added in the center of the feeding network, as shown in Fig. 3b , to account for the fabrication requirement of soldering the SMA connector pin to the two central microstrip lines. The four slot array elements excited by the quasi-TEM mode realized using PRGW technology are shown in Fig. 3c . The center-to-center distance between the slots is close to one wavelength at 10 GHz. Since the impedance matching of the slot antenna was insufficient to span the entire 8–12 GHz frequency range, a horn element was added to the antenna to improve the impedance matching and far-field parameters inspired by prior work on dipole-fed integrated horn antennas at millimeter-wave frequencies[4–6].

Horn antennas can be used to improve the antenna's gain, efficiency, and impedance bandwidth[4]. Therefore, an H-plane horn is presented here and placed on top of each slot element to control the side-lobe levels and improve the gain. Figure 4a shows the final design of the 2-by-2 H-plane horn slot antenna array with an aperture size of each horn element of $0.7\lambda_0 \times 0.38\lambda_0$, where λ_0 represents the wavelength in free space corresponding to the central frequency, to guarantee an element spacing of $0.7\lambda_0$ across the operating band, which is small enough to avoid grating lobes over a wide-band, optimizes overall impedance bandwidth, enhances the aperture phase uniformity, and consequently the antenna gain. The total size of the array is $1.6\lambda_0 \times 1.6\lambda_0$, which corresponds to $4.8 \times 4.8\ \mathrm{cm}^2$. Metallic blocks have been placed on the four sides of the antenna to hold up the top metal plane consisting of the slot and horn elements, as well as to make the fabrication process simpler.

Figure 4b shows the cross sections of the antenna, together with the details of the geometry of the horn element. The horn antenna increases the effective radiating aperture of the underlying slot antenna. The increased uniformity of the field distribution on the aperture of the horn, and the smoother impedance matching to free space compared to the slot, improve the overall gain and bandwidth. A modal analysis was carried out to verify that the horn dimensions are effective to propagate the first mode. Multiple modes can be excited on the slot due to reflection and scattering of the fields between the slot and the feed line. The slot supports propagation of the TE_{10} mode only, while higher order modes are evanescent, as shown in Fig. 5a . Without the horn, choosing larger slot sizes makes the matching to free space difficult and reduces the bandwidth. Therefore, the slot size is not increased any more, and the bottom aperture of the horn is selected to be larger than the slot length in the x-direction. This enables propagation of the TE_{10} mode only, as illustrated in Fig. 5b , via a direct coupling

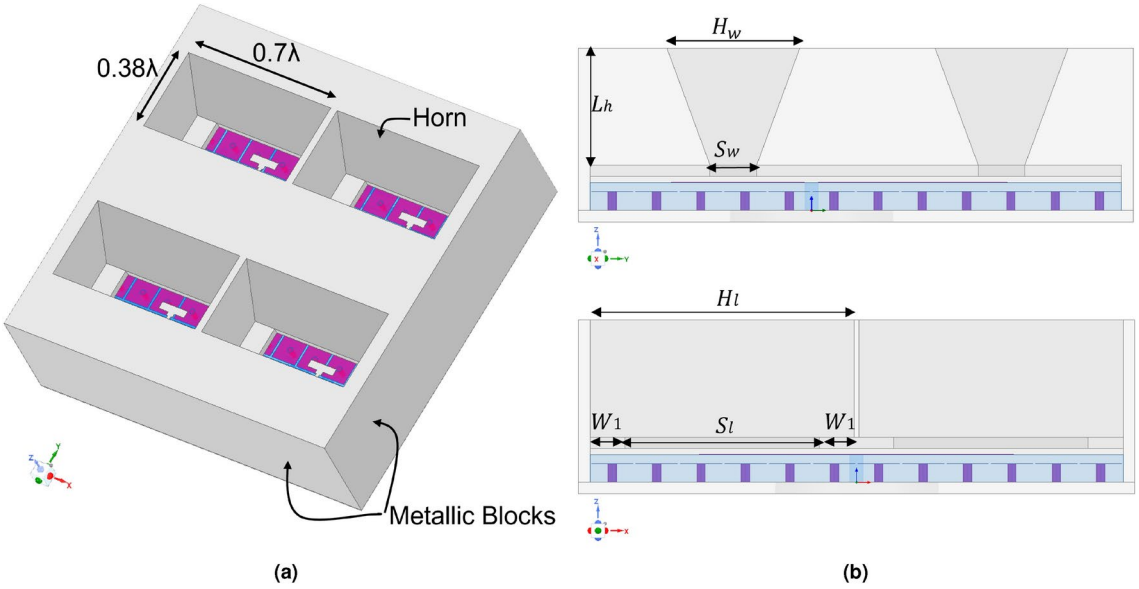

Fig. 4. Final geometry of the H-plane horn slot antenna array fed by PRGW. (**a**) 3D view, and (**b**) side views of the antenna with dimensions of $L_h = 10$ mm (height of horn), $H_w = 11.4$ mm (width of horn aperture), $H_l = 22$ mm (length of horn aperture), $S_w = 4$ mm (width of slot), and $S_l = 16$ mm (length of slot), $W_1 = 3$ mm.

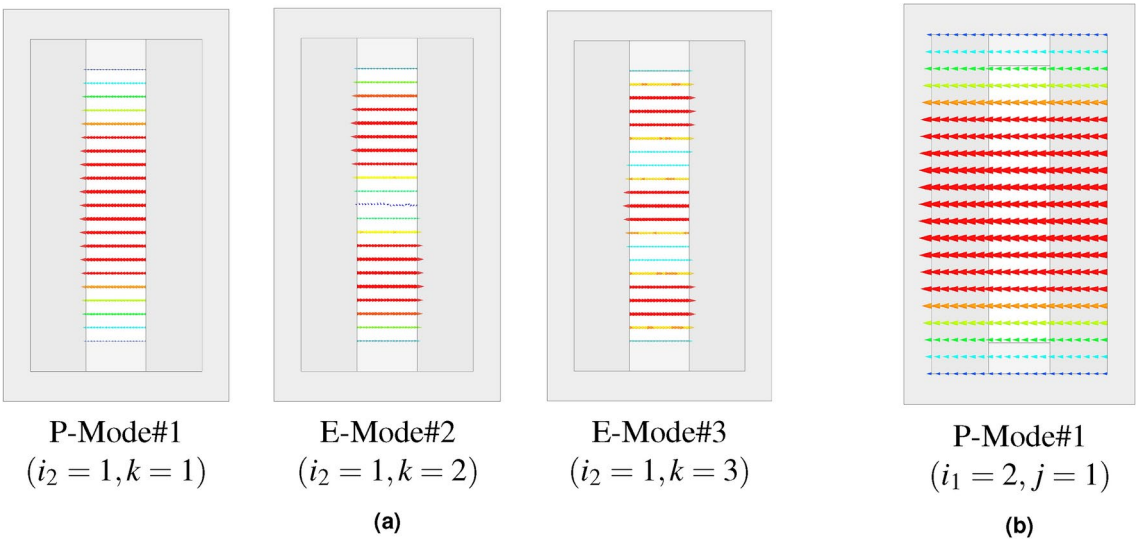

Fig. 5. (**a**) Excited P(propagating)- and E(evanescent)- modes on the slot aperture. (**b**) Propagating mode on the horn aperture. i_1 is the port number located on the horn aperture, whereas i_2 is the port number located on the slot aperture, and j and k are the orders of the modes excited on the horn aperture and the slot, respectively.

mechanism and creates a more uniform field distribution on the horn aperture, which increases the gain. The gradual impedance matching to free space, compared to the case of the slot without the horn, increases the frequency bandwidth.

Radiation of the second mode (TE_{20}) beyond the slot aperture opening in the *xy*-plane is given by

$$\vec{E} = \hat{y} E_0 \sin\left(2\pi \frac{x}{a}\right), \tag{1}$$

where *a* is the slot length (S_l) in the *x* direction.

Based on image theory, the field beyond the slot aperture can be evaluated by finding the radiation of the surface magnetic current ([36], Sec.3.6)

$$\vec{M}_s = 2\vec{E} \times \hat{z} = 2\hat{x}E_0 \sin\left(2\pi\frac{x}{a}\right), \tag{2}$$

in free space.

The far field is proportional to $\vec{L}$, which is given by

$$\vec{L} = \iint_{S_a} \mathrm{M}_s(r')e^{j\mathrm{k}r'\cos\psi} \cdot d\mathbf{S}', \tag{3}$$

where S_a refers to the aperture region, k denotes the propagation vector, and $r'\cos\psi = \mathbf{r}' \cdot \hat{r} = \hat{x}\sin\theta\cos\phi + \hat{y}\sin\theta\sin\phi$. Hence, from (2) and (3) we can evaluate L_x as

$$L_x = -\frac{2aE_0}{\pi k}\sin\left(\frac{ka}{2}\sin\theta\cos\phi\right)\frac{k\sin\theta\sin\phi}{\sin\theta\sin\phi} + \frac{2jkaE}{2\pi k}\frac{\cos\left(\frac{ka}{2}\sin\theta\cos\phi\right)\sin\left(\frac{kb}{2}\sin\theta\sin\phi\right)}{\pi^2 - (ka\sin\theta\cos\phi)^2}. \tag{4}$$

At broadside ($\theta = \phi = 0$), the field calculated from (4) is zero. This means that the second mode will create a null at broadside, thus, this should be suppressed as much as possible. Furthermore, by adding a horn on top of the slot, the second mode is suppressed further by keeping it in the evanescent state. At the same time, we try to avoid designing a long horn to keep the antenna low profile. As shown in Fig. 5b , the TE_{10} mode is the only propagating mode along the horn. As a result, the second mode will continuously decrease along the horn since the largest dimension of the horn (the top outer aperture) does not support the TE_{20} mode.

Figure 6 shows the comparison of the TE_{10} mode distribution using S-parameter coupling from the input port (P#1) to two cases: (i) a second port (P#2) on the slot aperture (without horn), and (ii) a second port on the horn aperture (with horn). The figure verifies that using a horn element improves the uniformity of the field distribution on the radiating aperture. Concerning the radiation through the horn elements, the height of the horn was chosen to be as small as possible (here, 10 mm equal to $\lambda_0/3$ at 10 GHz) to retain a low profile and maintain a small volume.

Experimental results

To validate the performance of the proposed 2-by-2 H-plane horn slot antenna array, the final design was fabricated as shown in Fig. 7 and tested. The feeding network was implemented using standard printed circuit technology on a PCB, shown in Fig. 7a . The input port was applied from the bottom using an SMA panel mount Jack connector with a 4-hole flange, with its center pin soldered to the pad connected to the microstrip lines. The slot plane and H-plane horns were made of copper and form the top metal layer, which is connected to the ground layer by using metallic blocks and screws at each of the four corners, as shown in Fig. 7b. The antenna metallic block was fabricated using a CNC milling machine. Figure 7c, d show the mounting of the AUT in the anechoic chamber, and the measurement setup, respectively.

The S_{11} was measured using an N5224B vector network analyzer. The simulated and measured reflection coefficients are compared in Fig. 8a. An impedance bandwidth of over 58.5% from 7 to 12.8 GHz is achieved, which is superior compared to a bandwidth of less than 25% for the antenna without the horns. Therefore, this demonstrates that by employing the H-plane horn element, the impedance matching is improved over a much larger frequency range. There is good agreement between the simulated and measured results of the horn slot antenna array, even though we observed that the matching is sensitive to the quality of the soldering

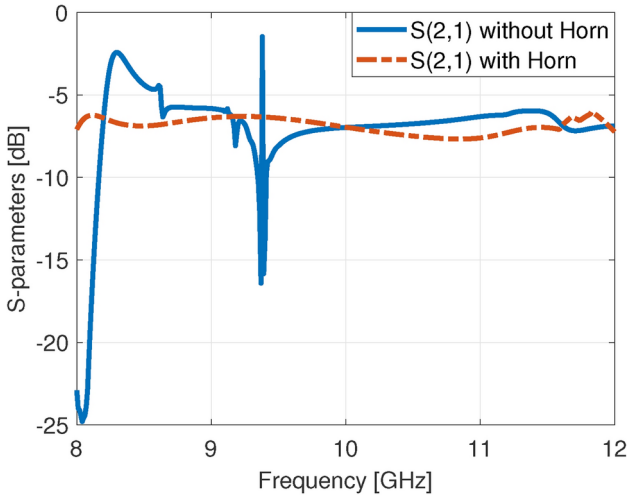

Fig. 6. Comparison of TE_{10} mode distribution using S-parameter coupling from the input port (P#1) to two cases: (i) a second port (P#2) on the slot aperture (without horn), and (ii) a second port (P#2) on the horn aperture (with horn).

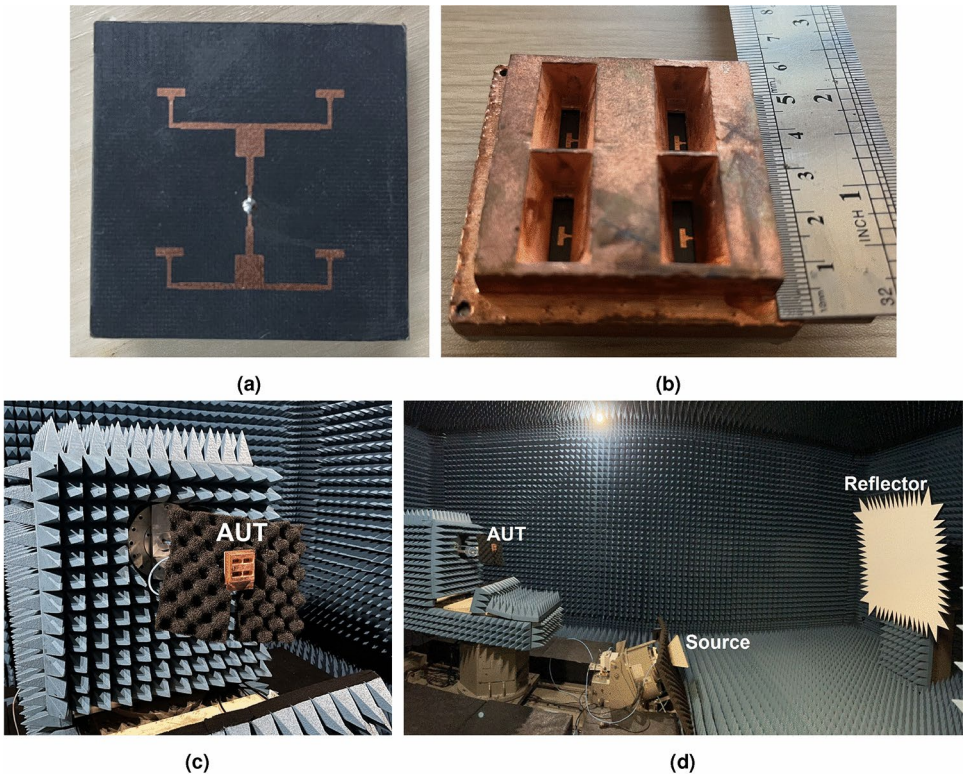

Fig. 7. (**a**) Fabricated prototype of the feeding network. (**b**) Final assembly of the 2-by-2 H-plane horn slot antenna array. (**c**) Antenna under test (AUT). (**d**) Measurement setup, where the antenna is tested in the receiving mode.

contact between the SMA connector and the feed line. The frequency shift between the simulated and measured reflection coefficients is mainly due to the manual soldering of the components and inherent PCB fabrication tolerances.

To measure the antenna gain, the gain comparison method was used by measuring the received power of the AUT and the received power of a reference standard-gain horn antenna, and computing the difference between the received power of both antennas. Figure 8b shows that the simulated and measured gain results are in very good agreement. The H-plane horn element increases the electrical length and effective aperture, and also improves the uniformity of the field distribution on the radiating aperture. All these desired changes improve the antenna gain at broadside by 3.1 dB compared to the antenna without the horn element, from 11 to 14.1 dBi at 10 GHz, and reduce the sidelobe and backlobe levels. Moreover, an enhanced gain stability for the horn slot configuration can be seen from 8 to 12 GHz. Figure 8c shows the measured and simulated radiation efficiency of the antenna. The simulated efficiency is above 94%, while the measured efficiency is above 86% over the whole X-band. The measured efficiency has been calculated by dividing the measured realized gain by the simulated directivity[37].

The comparison of the simulated and measured radiation patterns in both the E- and H-planes of the horn slot antenna array at various X-band frequencies are reported in Fig. 9a, b, respectively. The results, which are in very good agreement with the simulations, demonstrate stable radiation patterns in the entire frequency band. Also, the measured sidelobe levels in both the E- and H-planes are less than -15 dB and -10 dB over the entire frequency band, respectively. Additionally, the value of the cross-polarization in both planes is more than 30 dB below the main lobe over the whole frequency band.

Conclusion

In this work, an innovative 2-by-2 H-plane horn slot antenna array based on PRGW technology with a small size and very simple configuration is presented to operate at X-band frequencies. The most prominent advantage of PRGW compared to other technologies is low complexity in terms of design and fabrication and the reduction of the inter-element coupling effects. In the proposed design, using a symmetric feeding network and adding a compact H-plane horn element to each slot antenna increases the antenna's overall gain and bandwidth. The measurement results demonstrate good agreement with simulations over an impedance bandwidth of 58.5%, covering a band greater than the X-band frequency range. The antenna exhibits a measured gain of 14.1 dBi at the central operating frequency of 10 GHz, which is 3.1 dB higher than the antenna without the horn element. Additionally, the measured radiation efficiency is greater than 86% over the entire bandwidth. Based on these results, the H-plane horn slot antenna array presented in this work is suitable for use in a wide range of applications in the X-band, including wireless telecommunications, radar systems, and biomedical applications.

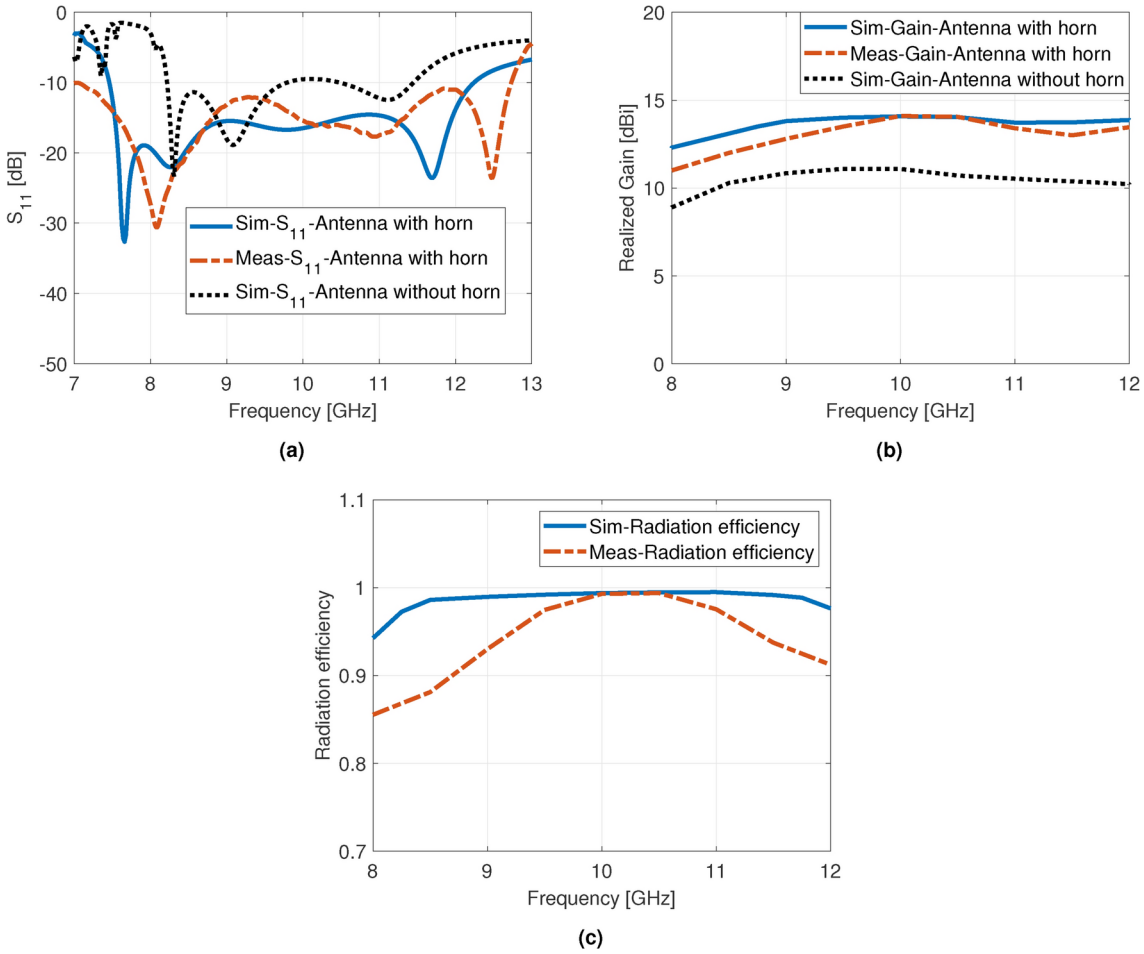

Fig. 8. Measured and simulated (**a**) S_{11}, (**b**) realized gain, and (**c**) radiation efficiency.

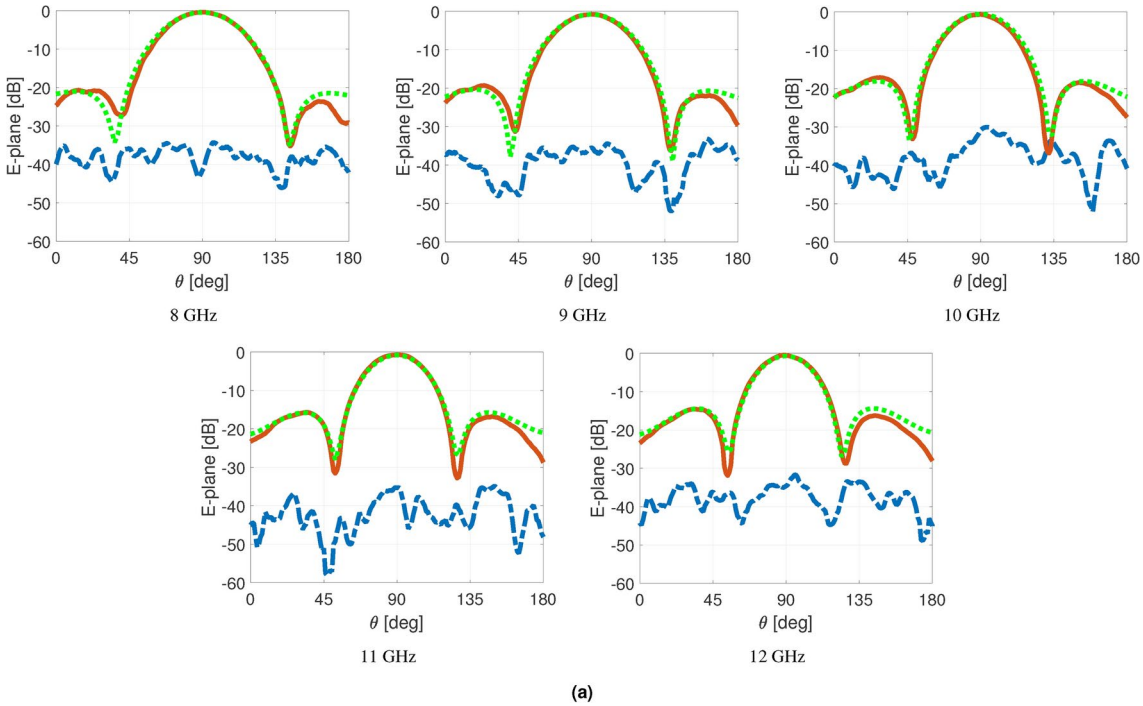

Fig. 9. Measured co- (red solid line), measured cross- (blue dashed line) and simulated co- (green dotted line) polarization radiation patterns of the H-plane horn slot antenna array in the (**a**) E- and (**b**) H-plane at 8, 9, 10, 11, and 12 GHz.

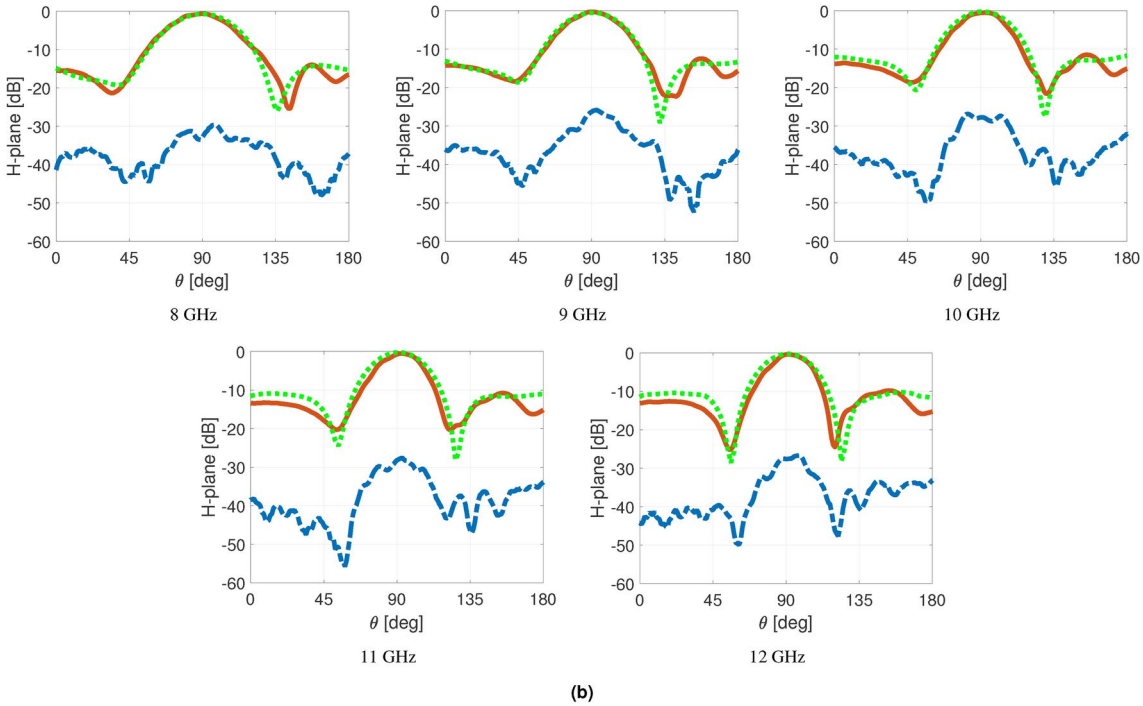

Figure 9. (continued)

Data availability

All data sets generated or analyzed during this study are available from the corresponding author upon reasonable request. Please, contact (mtaraji@torontomu.ca).

Received: 5 November 2024; Accepted: 21 April 2025
Published online: 21 May 2025

References

1. Arand, B. A. & Bazrkar, A. Design and implementation of a high efficiency microstrip array antenna for X-band monopulse tracking applications. *IET Microw. Antennas Propag.* **14**, 1272–1282 (2020).
2. Vaquero, Á. F., Rebollo, A. & Arrebola, M. Additive manufacturing in compact high-gain wideband antennas operating in mm-wave frequencies. *Sci. Rep.* **13**, 10998 (2023).
3. Zarifi, D., Saber, A. S. & Zaman, A. U. A high-gain gap waveguide-based 16×16 slot antenna array with low sidelobe level for mmwave applications. *Sci. Rep.* **14**, 31458 (2024).
4. Rebeiz, G. M., Katehi, L. P., Ali-Ahmad, W. Y., Eleftheriades, G. V. & Ling, C. C. Integrated horn antennas for millimeter-wave applications. *IEEE Antennas Propag. Mag.* **34**, 7–16 (1992).
5. Eleftheriades, G. V., Ali-Ahmad, W. Y., Katehi, L. P. & Rebeiz, G. M. Millimeter-wave integrated-horn antennas: Part I-theory. *IEEE Trans. Antennas Propag.* **39**, 1575–1581 (1991).
6. Ali-Ahmad, W. Y., Eleftheriades, G. V., Katehi, L. P. & Rebeiz, G. M. Millimeter-wave integrated-horn antennas: Part II-experiment. *IEEE Trans. Antennas Propag.* **39**, 1582–1586 (1991).
7. Levine, E., Malamud, G., Shtrikman, S. & Treves, D. A study of microstrip array antennas with the feed network. *IEEE Trans. Antennas Propag.* **37**, 426–434 (1989).
8. Pozar, D. Considerations for millimeter wave printed antennas. *IEEE Trans. Antennas Propag.* **31**, 740–747 (1983).
9. Li, M. & Luk, K.-M. Low-cost wideband microstrip antenna array for 60-GHz applications. *IEEE Trans. Antennas Propag.* **62**, 3012–3018 (2014).
10. Lak, A., Adelpour, Z., Oraizi, H. & Parhizgar, N. Design and SAR assessment of three compact 5G antenna arrays. *Sci. Rep.* **11**, 21265 (2021).
11. Sehrai, D. A. et al. Design of high gain base station antenna array for mm-wave cellular communication systems. *Sci. Rep.* **13**, 4907 (2023).
12. Miura, Y., Hirokawa, J., Ando, M., Shibuya, Y. & Yoshida, G. Double-layer full-corporate-feed hollow-waveguide slot array antenna in the 60-GHz band. *IEEE Trans. Antennas Propag.* **59**, 2844–2851 (2011).
13. Wu, J., Cheng, Y. J. & Fan, Y. A wideband high-gain high-efficiency hybrid integrated plate array antenna for V-band inter-satellite links. *IEEE Trans. Antennas Propag.* **63**, 1225–1233 (2014).
14. Zhao, Y. & Luk, K.-M. Dual circular-polarized SIW-fed high-gain scalable antenna array for 60 GHz applications. *IEEE Trans. Antennas Propag.* **66**, 1288–1298 (2018).
15. Wang, L., Gómez-Tornero, J. L. & Quevedo-Teruel, O. Substrate integrated waveguide leaky-wave antenna with wide bandwidth via prism coupling. *IEEE Trans. Microw. Theory Tech.* **66**, 3110–3118 (2018).
16. Li, T. & Chen, Z. N. Control of beam direction for substrate-integrated waveguide slot array antenna using metasurface. *IEEE Trans. Antennas Propag.* **66**, 2862–2869 (2018).
17. Cheng, Y. J., Hong, W. & Wu, K. 94 GHz substrate integrated monopulse antenna array. *IEEE Trans. Antennas Propag.* **60**, 121–129 (2011).
18. Han, W., Yang, F., Ouyang, J. & Yang, P. Low-cost wideband and high-gain slotted cavity antenna using high-order modes for millimeter-wave application. *IEEE Trans. Antennas Propag.* **63**, 4624–4631 (2015).

19. Li, Y. & Luk, K.-M. 60-GHz substrate integrated waveguide fed cavity-backed aperture-coupled microstrip patch antenna arrays. *IEEE Trans. Antennas Propag.* **63**, 1075–1085 (2015).
20. Kildal, P.-S., Alfonso, E., Valero-Nogueira, A. & Rajo-Iglesias, E. Local metamaterial-based waveguides in gaps between parallel metal plates. *IEEE Antennas Wirel. Propag. Lett.* **8**, 84–87 (2008).
21. Kildal, P.-S. Three metamaterial-based gap waveguides between parallel metal plates for mm/submm waves. In *2009 3rd European Conference on Antennas and Propagation*, 28–32 (2009).
22. Taraji, M. & Naser-Moghaddasi, M. Design of branch line coupler based on ridge gap waveguide technology for X-band application. *IETE J. Res.* **68**, 917–923 (2019).
23. Ferrando-Rocher, M. et al. 8×8, Ka-band dual-polarized array antenna based on gap waveguide technology. *IEEE Trans. Antennas Propag.* **67**, 4579–4588 (2019).
24. Vosoogh, A., Brazález, A. A. & Kildal, P.-S. A V-band inverted microstrip gap waveguide end-coupled bandpass filter. *IEEE Microw. Wirel. Compon. Lett.* **26**, 261–263 (2016).
25. Zaman, A. U. & Kildal, P.-S. Wide-band slot antenna arrays with single-layer corporate-feed network in ridge gap waveguide technology. *IEEE Trans. Antennas Propag.* **62**, 2992–3001 (2014).
26. Razavi, S. A., Kildal, P.-S., Xiang, L., Alos, E. A. & Chen, H. 2×2-slot element for 60-GHz planar array antenna realized on two doubled-sided PCBs using SIW cavity and EBG-type soft surface fed by microstrip-ridge gap waveguide. *IEEE Trans. Antennas Propag.* **62**, 4564–4573 (2014).
27. Pucci, E., Rajo-Iglesias, E., Vazquez-Roy, J.-L. & Kildal, P.-S. Planar dual-mode horn array with corporate-feed network in inverted microstrip gap waveguide. *IEEE Trans. Antennas Propag.* **62**, 3534–3542 (2014).
28. Sorkherizi, M. S., Dadgarpour, A. & Kishk, A. A. Planar high-efficiency antenna array using new printed ridge gap waveguide technology. *IEEE Trans. Antennas Propag.* **65**, 3772–3776 (2017).
29. Sifat, S. M., Ali, M. M. M., Shams, S. I. & Sebak, A.-R. High gain bow-tie slot antenna array loaded with grooves based on printed ridge gap waveguide technology. *IEEE Access* **7**, 36177–36185 (2019).
30. Dadgarpour, A., Bayat-Makou, N., Antoniades, M. A., Kishk, A. A. & Sebak, A. A dual-polarized magnetoelectric dipole array based on printed ridge gap waveguide with dual-polarized split-ring resonator lens. *IEEE Trans. Antennas Propag.* **68**, 3578–3585 (2020).
31. Taraji, M. & Antoniades, M. A. Design of a compact 2-by-2 horn slot antenna array fed by printed ridge gap waveguide. In *2023 IEEE International Symposium on Antennas and Propagation and USNC-URSI Radio Science Meeting (USNC-URSI)*, 1657–1658 (2023).
32. Valero-Nogueira, A., Alfonso, E., Herranz, J. I. & Kildal, P.-S. Experimental demonstration of local quasi-TEM gap modes in single-hard-wall waveguides. *IEEE Microw. Wirel. Compon. Lett.* **19**, 536–538 (2009).
33. Mahmud, R. H. & Lancaster, M. J. A 2×2 filtering subarray element antennas using all-resonator structures. *IET Microw Antennas Propag.* **15**, 592–599 (2021).
34. Jung, E.-Y., Lee, J. W., Lee, T. K. & Lee, W.-K. SIW-based array antennas with sequential feeding for X-band satellite communication. *IEEE Trans. Antennas Propag.* **60**, 3632–3639 (2012).
35. Polemi, A., Maci, S. & Kildal, P.-S. Dispersion characteristics of a metamaterial-based parallel-plate ridge gap waveguide realized by bed of nails. *IEEE Trans. Antennas Propag.* **59**, 904–913 (2010).
36. Jin, J.-M. *Theory and Computation of Electromagnetic Fields* (Wiley, New York, 2015).
37. Yektakhah, B. & Sarabandi, K. A wideband circularly polarized omnidirectional antenna based on excitation of two orthogonal circular TE_{21} modes. *IEEE Trans. Antennas Propag.* **65**, 3877–3888 (2017).

Acknowledgements

This work was supported in part by the Natural Sciences and Engineering Research Council (NSERC) of Canada, in part by the Canada Foundation for Innovation (CFI), and in part by CMC Microsystems.

Author contributions

M. Taraji designed and simulated the antenna, and performed the measurements. All authors discussed the results and reviewed the manuscript. M. A. Antoniades and E. Baladi provided overall supervision and guidance.

Declarations

Competing interests

The authors declare no competing interests.

Additional information

Correspondence and requests for materials should be addressed to M.T.

Reprints and permissions information is available at www.nature.com/reprints.

Publisher's note Springer Nature remains neutral with regard to jurisdictional claims in published maps and institutional affiliations.